

Ghost-dil-NetVLAD: A Lightweight Neural Network for Visual Place Recognition

Qingyuan Gong^a, Yu Liu^a, Liqiang Zhang^{a,*} and Renhe Liu^a

^a*School of Microelectronics, Tianjin University, Tianjin, China*

ARTICLE INFO

Keywords:

Dilated convolution; Ghost module; low computational cost; lightweight CNN; visual place recognition;

ABSTRACT

Visual place recognition (VPR) is a challenging task with the unbalance between enormous computational cost and high recognition performance. Thanks to the practical feature extraction ability of the lightweight convolution neural networks (CNNs) and the train-ability of the vector of locally aggregated descriptors (VLAD) layer, we propose a lightweight weakly supervised end-to-end neural network consisting of a front-ended perception model called GhostCNN and a learnable VLAD layer as a back-end. GhostCNN is based on Ghost modules that are lightweight CNN-based architectures. They can generate redundant feature maps using linear operations instead of the traditional convolution process, making a good trade-off between computation resources and recognition accuracy. To enhance our proposed lightweight model further, we add dilated convolutions to the Ghost module to get features containing more spatial semantic information, improving accuracy. Finally, rich experiments conducted on a commonly used public benchmark and our private dataset validate that the proposed neural network reduces the FLOPs and parameters of VGG16-NetVLAD by 99.04% and 80.16%, respectively. Besides, both models achieve similar accuracy.

1. Introduction

Visual place recognition (VPR) plays an incredible role in robotics and localization in recent years. VPR significantly contributes to the mission of identifying a single localization or simultaneous localization and mapping (SLAM) systems [1]. Typically, The VPR problem can be formulated as image retrieval in an image database. To address the problem, a two-stage pipeline can be used: (1) extracting the vector representation from each image; (2) measuring the similarity between the query and each image in the database by a scoring function (e.g., Euclidean distance or cosine similarity) [2].

Currently, the most effective feature extraction method (first step) in VPR is to use deep learning techniques. The original design goal of a convolutional neural network (CNN) is to create a network in which neurons in the first layer extracts local visual features, and neurons in the last layer fuse these features to form higher-order features. CNN can compress a large-size raw image to small-dimension data to retain practical image features. Generally, to obtain better performance, the number of layers of the network is constantly increasing [3], from AlexNet [4] (7 layers) to VGG16 [5] (16 layers), and then to ResNet [6] with 152 layers.

However, more convolution layers mean more computational resources and memories. Although the network performance can be improved, efficiency issues follow. Hence, various lightweight models emerge for simplifying the calculations and adapting the embedded devices. For efficiency

issues, the usual method is to perform model compression. Compared with compressing a model, designing a lightweight model is a different approach: a more efficient network calculation method (mainly for the convolution method) is used to reduce model parameters with minor performance loss. For instance, GhostNet [7] utilized cheap operations (linear transformations) to generate feature maps instead of processing images by convolution operations, which could reveal important information underlying intrinsic features.

Further, the critical point to improving VPR performance after feature extraction is to form the compact global image representation when subjected to various image transformations (second step) [8, 9]. VPR mission aggregates the extracted local feature descriptors to the global feature representations. The global descriptors [10] can be aggregated by bag-of-word (BoW), Fisher Vector (FV) and vector of locally aggregated descriptors (VLAD), etc. BoW uses the nearest neighbour cluster centers to represent feature points. FV clusters the data by Gaussian mixture model and then use the linear combination of all cluster centers to approximate feature points. VLAD is a popular descriptor pooling method, for instance, level retrieval [11, 12]. It captures information about the statistics of local descriptors aggregated over the image and stores the sum of residuals (difference vector between the descriptor and its corresponding cluster center) for each visual word. However, features extracted by these methods are all handcrafted and not robust enough to the environmental changes such as lighting conditions, scales and viewpoints. Inspired by VLAD, a novel CNN-based architecture, VGG16-NetVLAD, was design to mimic it [9]. It regards the output (i.e., $K \times W \times H$ feature map) of the front-ended CNN as $W \times H$ local descriptors with the length of K . It aggregates them with a specifically designed pooling layer to obtain the final global representation. Experimental results show its excellent performance on

* e-mail: gqy970506@tju.edu.cn; liuyu@tju.edu.cn; zhangliqiang@tju.edu.cn

** This research is supported by National Natural Science Foundation of China (61771338).

*Corresponding author

ORCID(s): 0000-0002-5949-6587 (Y. Liu); 0000-0003-2475-9268 (L. Zhang)

challenging public VPR dataset such as Pitts30k [13]. However, its computational cost is considerable.

Our main contributions in designing a VPR model with fast computational speed and high accuracy can be summarized as follows:

- we design a lightweight VPR model named Ghost-dil-NetVLAD with dilated convolution-based Ghost modules and a learn-able VLAD layer;
- we establish and open a location dataset of the Tianjin University campus named TJU-Location Dataset, including images of 50 iconic locations. In addition, a public dataset named Pitts30k is also used to discuss the performance of the proposed model and several VPR models.

The remaining framework of this paper is as follows: related works are presented in Section II. In Section III, we propose a lightweight model named Ghost-dil-NetVLAD. Section IV contains the experimental results and the ablation experiments of different fusion methods. The last section is the conclusion.

2. Related work

2.1. Lightweight VPR Model

Feature extraction is the first step in the VPR mission. The traditional feature representations include scale-invariant feature transform (SIFT), FAB-MAP and Cross-Region-BoW, improving the robustness against appearance or illumination changes. However, these methods always lead to a large amount of calculation compared to feature extracted by deep learning methods. Khaliq *et al.* [14, 15] propose two lightweight VPR methods: CAMAL and Region-VLAD. The CAMAL captures multi-layer context-aware attentions robust under changing environments and viewpoints. The Region-VLAD employs middle convolutional layers of AlexNet365 to process regional vocabulary and extraction of VLAD for image matching. Although these methods realize lightweight structures, the convolutional structure of the front-end CNN is not optimized. Therefore, it still leads to considerable computational cost.

2.2. Deep Learned Representations for VPR

For VPR tasks, CNNs are specialized for processing images or videos [11]. With the excellent performance of CNNs in the field of vision classification and segmentation in recent years, it has been shown that the image representations generated by CNNs can be transferable to other visual tasks. In other words, the feature extracted from CNNs can also be applied to image retrieval tasks to achieve good results. Namely, the feature extracted by CNNs is robust and discriminative in changing environments [4]. Babenko *et al.* [16] propose that the feature map with a size of $H \times W \times C$ generated by CNNs for image classification obtains impressive results as representations in the VPR task. Simply flattening the feature maps of a convolution layer does not take

full advantage of the spatial information [17]. Therefore, improving the current state-of-the-art representations for visual place recognition can add aggregated representations layers behind the feature maps.

The aggregated representation layers can be seen as an $H \times W$ grid of C -dimensional feature descriptors to a vector representing the original image, aggregating local features into a representative global feature. And then, a similarity function (e.g., Euclidean distance or cosine similarity) is leveraged to select the best candidate for image retrieval. There are many classic algorithms about image vector aggregating, e.g., VLAD [18], BoW [19], Fisher vector [20] and aggregated selective matching kernel (ASMK) [21]. However, these algorithms are not robust enough to environmental changes such as lighting conditions, scales and viewpoints. Thanks to the development of deep learning technology, a model named NetVLAD implements the VLAD layer embedding and aggregation behind the CNN structure for VPR [9]. In recent years, [22–25] improve the origin NetVLAD model with the process of changing the loss function or adding feature matching to enhance the performance. Nevertheless, none of them considers the computing power required by the actual operation of the model and the potentiality of these models adapted to embedded devices. [9]. In recent years, [22–25] improve the origin NetVLAD model with the process of changing the loss function or adding feature matching to enhance the performance. Nevertheless, none of them considers the computing power required by the actual operation of the model and the potentiality of these models adapted to embedded devices.

2.3. Lightweight CNN

There are two main methods of lightening neural networks: model compression and compact model design. Model compression includes binarization methods, tensor decomposition, and knowledge distillation, etc. They can accelerate the model by efficient binary operations, exploit the redundancy and low-rank property in parameters, or utilize larger models to teach smaller ones. In addition, these methods can not fundamentally improve the lightweight degree of the model. The improvement on basic operations and architectures will make them go further [7].

There are many lightweight CNN models by a compact model design, like MobileNets and ShuffleNet, etc. MobileNetV1 [26] is first proposed by Google. It is of small size and low calculation, suitable for mobile devices. It is lightweight, using depthwise separable convolution instead of standard convolution, and uses width multiply to reduce parameters. MobileNetV2 [27] proposes inverted residual block, and MobileNetV3 [28] further utilizes AutoML technology, achieving better performance with fewer floating-point operations (FLOPs). ShuffleNet [29] is a lightweight network structure proposed by Face++. The main thought is to use Group convolution and Channel shuffle to improve ResNet, regarded as a compressed version of ResNet. ShuffleNetV2 [30] introduces channel split operation to realize fast and high precision. GhostNet [7] uses a series of sim-

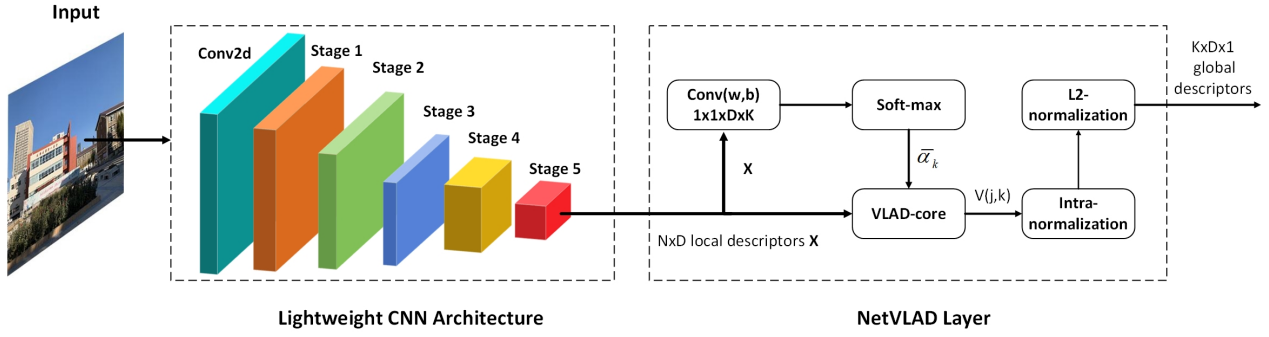


Figure 1: The proposed framework for place recognition. The feature extraction part is lightweight CNN architecture, which is a 5-stage CNN architecture. Through every stage, the feature map becomes a half one. The NetVLAD layer processes local descriptors to global descriptors.

ple linear transformations with cheap cost to generate ghost feature maps that could fully reveal information underlying intrinsic features. In efficiency and accuracy, GhostNet is better than others. In the work of GhostNet, the Ghost module is introduced and can be taken as a plug-and-play component.

3. Methodology

The framework of our proposed Ghost-dil-NetVLAD is shown in Fig. 1. The Ghost-dil-NetVLAD contains two parts. One is the lightweight feature extraction architecture (GhostCNN) shown in Section 3.1, and the remaining is the NetVLAD layer described in Section 3.2.

3.1. GhostCNN

For the traditional CNN, the redundancy in feature maps always guarantees a comprehensive understanding of the input data. For example, there are many similar feature maps through the convolution layer of ResNet [6], just like ghosts of each other. The redundancy in feature maps is an essential feature for the success of deep neural networks. However, it results in massive computational costs. Inspired by basic Ghost modules in the GhostNet [7], we design the lightweight neural network named GhostCNN for front-ended feature extraction. Ghost modules skillfully utilize linear transformations to generate ghost feature map pair examples to reduce the computational cost significantly and ensure a satisfactory accuracy simultaneously. The proposed GhostCNN consists of a convolution operation and five stages. After each step, the size of the output feature maps are reduced by half till the stage 4. There are at least two Ghost bottlenecks [7] in each stage, and each bottleneck contains two Ghost modules (its architecture is shown in Fig. 3). The detailed architecture of the GhostCNN is given in Table 1.

3.1.1. Ghost Bottleneck

Similar to the basic residual block in ResNet, the Ghost bottleneck consists of two stacked Ghost modules, as shown in Fig. 2. The first Ghost module is used as an expansion layer, increasing the number of channels, and the second

Table 1
GhostCNN architecture.

Stage	output size	Operator	Stride	SE
-	320x240x24	Conv2d 3x3	2	0
stage1	160x120x40	Ghost bottleneck	1	0
		Ghost bottleneck	2	0
stage2	80x60x112	Ghost bottleneck	1	0
		Ghost bottleneck	2	1
stage3	40x30x160	Ghost bottleneck	1	1
		Ghost bottleneck	2	0
stage4	20x15x960	Ghost bottleneck	1	0
		Ghost bottleneck	1	0
		Ghost bottleneck	1	0
		Ghost bottleneck	1	1
		Ghost bottleneck	1	1
		Ghost bottleneck	2	1
stage5	20x15x960	Ghost bottleneck	1	0
		Ghost bottleneck	1	1
		Ghost bottleneck	1	0
		Ghost bottleneck	1	1

Ghost module reduces the number of channels to match the shortcut. Then, the input and the result from the second Ghost module are fed into the shortcut connection to generate the final output. If Stride=2, a depthwise convolution

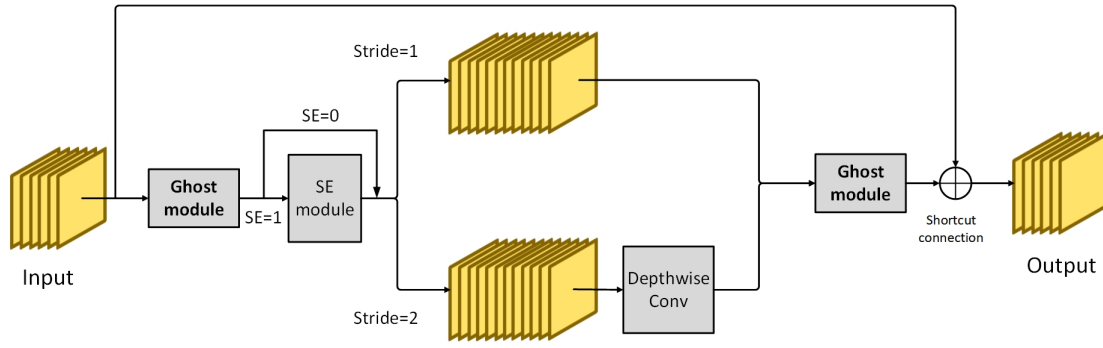


Figure 2: Ghost bottleneck architecture.

layer is inserted between the two Ghost modules. Depthwise convolution processes the image from each channel simultaneously, and the number of feature maps after this operation is the same as the number of input channels. If $SE=1$, the squeeze-and-excitation (SE) module is selected. The SE block [31] comprises an average pooling layer and two point-wise convolutions. It is implemented to enhance the channelwise feature responses.

3.1.2. Ghost Module

First, given the input data $X \in \mathbb{R}^{c \times h \times w}$, m feature maps ($Y \in \mathbb{R}^{h \times w \times m}$ where h and w are the height and width of the input data, respectively) can be generated using

$$Y = X * f \quad (1)$$

where $f \in \mathbb{R}^{c \times k \times k \times m}$ is the convolution filter with the kernel size of $k \times k$; c is the number of input channels. For the traditional CNN, the original number of intrinsic feature maps is D . But after this step, the number of output feature maps is m ($m \leq D$).

Second, cheap operation (i.e., Eq. 2) including identity transformation is performed on each feature map in Y to obtain the desired n feature maps. Each feature map in Y generates s ghost feature maps, a total of $m \times s$, to ensure that the feature map shape of the Ghost module and the standard convolution output is the same.

$$y_{ij} = \Phi_{i,j}(y_i), \quad \forall i = 1, \dots, m, \quad j = 1, \dots, s \quad (2)$$

where y_i is the i -th intrinsic feature map in Y , $\Phi_{i,j}$ is the j -th linear operation (except the last one) to generate the j -th ghost feature map y_{ij} . Namely, y_i can have one or more ghost feature maps $\{y_{ij}\}_{j=1}^s$. The last $\Phi_{i,s}$ is the identity mapping for preserving the intrinsic feature maps. Through Eq. 2, we have $D = m \times s$ feature maps. $Y' = [y_{11}, y_{12}, \dots, y_{ms}]$ as the output data of a Ghost module.

From Fig. 3, the dilated convolution part shows the different receptive fields of convolution filter with different dilated rates. For different dilated rates, the number of parameters associated with each layer is identical. Intuitively, when multiple convolution kernels with different dilation rates are superimposed, other receptive fields will bring multi-scale context information. Therefore, we add dilated convolutions

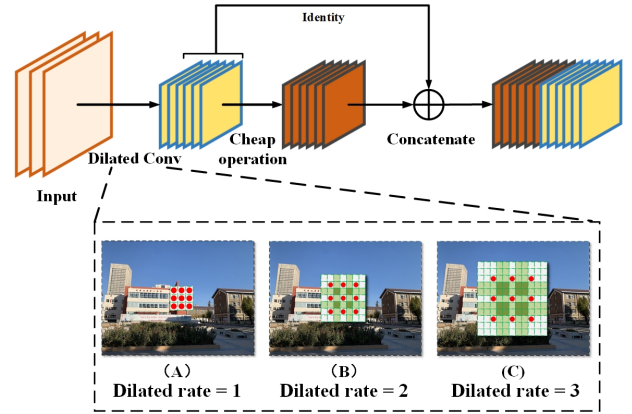


Figure 3: Ghost module with dilated convolution filter. We add dilated convolutions to the first step of the Ghost module. Sub-figure (A) shows the 3×3 receptive field of 1-dilated convolution filter (i.e., ordinary convolution). (B) reveals the 7×7 receptive field of 2-dilated convolution filter. (C) indicates the 11×11 receptive field of 3-dilated convolution filter.

in the Ghost module to improve the model performance. Dilated convolutions support an exponential expansion of the receptive field, which means that the output feature maps contain more global features and semantically higher-level features. It is conducive to the image recognition task.

3.2. NetVLAD layer

Vector of locally aggregated descriptors (VLAD) [32] store the sum of residuals (difference vector between the descriptor and its corresponding cluster center) for each visual word. The NetVLAD [9] uses the CNN architecture to capture the information about the statistics of local descriptors aggregated over the image. Given the input image I , the local descriptor Y' can be obtained by

$$f_{GhostCNN} : I \rightarrow Y' \in \mathbb{R}^{h \times w \times D} \quad (3)$$

In other words, the output of GhostCNN's last convolution layer is a $h \times w \times D$ feature map which can be considered as a set of D -dimensional descriptors extracted at $h \times w$ spatial locations. Similarly, the feature map can be deemed as N ($N = h \times w$) D -dimensional feature descriptors $\{\mathbf{x}_i\}_{i=1}^N$ with

each of them representing the local features at specific local positions of the input image.

Formally, given local image descriptors $\{\mathbf{x}_i\}_{i=1}^N$ as input, and cluster centers (visual words) $\{\mathbf{c}_k\}_{k=1}^K$ as VLAD parameters, the output VLAD image representation V is $D \times K$ -dimensional. The (j, k) element of V can be expressed by

$$V(j, k) = \sum_{i=1}^N \bar{\alpha}_k(\mathbf{x}_i) (x_i(j) - c_k(j)) \quad (4)$$

where $x_i(j)$ is the j -th dimensions of the i -th descriptor and $c_k(j)$ denotes the k -th cluster center; $\bar{\alpha}_k(\mathbf{x}_i)$ is the weight between the descriptor \mathbf{x}_i and the k -th cluster center. The weight ranges from 0 to 1, with the highest weight assigned to the closest cluster center. Namely, $\bar{\alpha}_k(\mathbf{x}_i)$ is 1 if cluster \mathbf{c}_k is closest to the descriptor \mathbf{x}_i and 0 otherwise. $\sum_{k=1}^K \bar{\alpha}_k(\mathbf{x}_i) = 1$. The weight is trainable via back-propagation and can be described as follows

$$\bar{\alpha}_k(\mathbf{x}_i) = \frac{e^{\alpha \|\mathbf{x}_i - \mathbf{c}_k\|^2}}{\sum_{k'} e^{-\alpha \|\mathbf{x}_i - \mathbf{c}_{k'}\|^2}} \quad (5)$$

which assigns the weight of descriptor \mathbf{x}_i to cluster \mathbf{c}_k according to their proximity.

For convenience, the output VLAD image representation V is written as a $D \times K$ matrix, and this matrix is reshaped into a row vector. After normalization, we have a $(K \times D) \times 1$ image representation. Then, the dimension reduction is performed using principal component analysis (PCA) with whitening followed by L2-normalization [33].

4. Experiments

This section describes our used datasets (Section 4.1) and evaluation metrics (Section 4.2). Finally, we perform quantitative and qualitative experiments to validate our proposed approach (Section 4.3).

4.1. Datasets

First, we leverage a commonly used public dataset (*Pitts30k-train*) to train our model. Then, a publicly available dataset (*Pitts30k-test*) and our established dataset (*TJU-Location*) are used to verify our method.

- *Pitts30k* [9, 13]: It is a public dataset containing 30 k database images downloaded from Google Street View and 22 k test queries captured at different times. The dataset is divided into three roughly equal parts for training, validation, and testing. Street views in the three sets are geographically disjoint. Each set contains 10 k images to process and 8 k queries, and the queries are geographically disjoint with the processed images.
- *TJU-Location*: As shown in Fig. 4, our dataset contains multiple street-level images taken at different times.



Figure 4: TJU-Location dataset examples. Each column shows perspective images taken at different times.

We selected 50 positions with distinctive characteristics of the buildings on the Weijin campus of Tianjin University. All points are isolated geographically. We recorded images from these locations by two smartphones (i.e., iPhone XR and Huawei Mate 20). In one place, images were taken per 45 degrees in the horizontal plane. In one horizontal direction, two images with different pitch angles were captured. We collected images in one location at 9:00 and 14:00, respectively. Therefore, 64 images were recorded at each location. Finally, a database containing 3.2 k images with 2.3 k queries was established. We split all database images into three roughly equal parts for training, validation, and testing. These subsets were independent of each other geographically. To obtain accurate positions of the collected images, we used the portable positioning module called Qianxun magic cube MC120M with sub-meter accuracy from Qianxun spatial intelligence company. We uploaded entire dataset to Baidu cloud disk and opened it.

(<https://pan.baidu.com/s/1F-uLbLUiD2rCmsXcN73uFw> and the code is 8wyd)

4.2. Evaluation Metrics

For all the datasets, they are evaluated using the Recall@N. The Recall quantifies the number of positive class predictions made out of all positive examples in the dataset. That is, the correct prediction is the proportion of all positive samples. The query image is correctly localized if at least one of the top N images is within the ground-truth tolerance. The queries are correctly recognized (positive proportion) if database images are retrieved within a specific range from true positions (GNSS positions).

In addition, model size and computing power requirements are essential indexes to evaluate the potential of deep learning models to be deployed in embedded systems. Therefore, two metrics, model parameters and FLOPs are introduced. Model parameters are used to reveal the model's complexity, and FLOPs reflect requirements for hardware such as GPU.

4.3. Implementation Details

All models were implemented on the publicly available PyTorch framework. Two NVIDIA Tesla V100 GPUs were leveraged for training, validation, and testing. In addition, we used stochastic gradient descent (SGD) as an optimizer. Its starting learning rate is 1×10^{-4} , and the parameter "weight_decay" is 1×10^{-3} . The batch size is 4 and the momentum is 0.9. For preprocessing, all images were resized to 640×480 pixels.

We used three representative CNN architectures (i.e., Alex-Net, VGG-16 and MobileNetV3) and our proposed GhostCNN as front-ends to extract feature maps. AlexNet and VGG-16 are cropped at the last convolution layer (conv5) with the encoder dimension (i.e., D -dimension) of 256 and 512 before ReLU, respectively. MobileNetV3 is cropped at the last stage with the encoder dimension of 960 before adaptive average pooling layer.

To train high-performance models, we used the triplet loss [9] as the loss function. The function consists of a triplet tuple $(q, \{p_i^q\}, \{n_j^q\})$, where $\{p_i^q\}$ is a set of potential positives (geographical distance within a specific range) and $\{n_j^q\}$ is a set of definite negatives (geographical distance a specific range). First, we need to choose the best positive ($p_{i*}^q = \arg\min_{\theta}(q, p_i^q)$). Namely, for a given test query image q , we wish that the euclidean distance between the query q and the best potential positive to be smaller than its distance to definite negative, which is described as

$$d_{\theta}(q, p_{i*}^q) < d_{\theta}(q, n_j^q), \forall j \quad (6)$$

Through the above inequality relationship, the loss function L_{θ} can be described as:

$$L_{\theta} = \sum_j l(\min_i (d_{\theta}^2(q, p_i^q)) + m - d_{\theta}^2(q, n_j^q)) \quad (7)$$

where m is a constant parameter as 0.1 to ensure that the query is close to the potential positive and away from the definite negative; l is the hinge loss $l(x) = \max(0, x)$.

Pre-train In NetVLAD [9], VGG-16 and AlexNet are pre-trained by ImageNet [34] for classification, which demonstrates that the end-to-end model achieves higher accuracy and training speed [35, 36]. The Imagenet dataset has more than 14 million images, covering more than 20000 categories, and it is widely used for deep learning perception. Nevertheless, most categories are objects and creatures. However, these images lack the point, line and angle features in the building images. Since we live in various buildings, more building features help improve the VPR model performance. Therefore, we pre-train all models on the Places-365 dataset [37] to ensure that they are sensitive to building features. Places-365 is a dataset for building classification and scene recognition. It has more than 18 million training images, with the image number per class varying from 3068 to 5000 for 365 categories. The validation set has 50 images per class, and the test set has 900 images per class.

4.4. Results and Discussion

In this section, five models including Alex-NetVLAD, VGG16-NetVLAD, MobileNetV3-NetVLAD, Ghost-NetVLAD (the Ghost module does not have dilated convolutions) and Ghost-dil-NetVLAD are trained on the Pitts30k-train dataset, and evaluated on the Pitts30k test and TJU-Location test datasets. Sufficient experiments are performed to discuss different model performances.

4.4.1. Model Accuracy

Table 2 shows the Recall@N of five models on the Pitts30k test dataset and TJU-Location test dataset. The experimental results demonstrate that VGG16-NetVLAD and Ghost-dil-NetVLAD achieve the best and second-best performance on the Pitts30k test dataset. The effects on the TJU-Location test dataset show that most Recall@N of Ghost-dil-NetVLAD are greater than those of the remaining models, which validates better generalization of GhostNet-dil-NetVLAD. Although our proposed lightweight GhostCNN omits many convolution processing, it still achieves satisfactory accuracy in VPR tasks. Compared with the lightweight MobileNetV3, GhostCNN preserves more redundancy in feature maps.

4.4.2. Model Efficiency

As shown in Fig. 5, it is evident that Ghost-NetVLAD outperforms other models in FLOPs and model parameters. There are few differences between Ghost-dil-NetVLAD and Ghost-NetVLAD in the model efficiency. However, VGG16-NetVLAD needs the most computational resources, which is not conducive to its deployment in embedded devices. Ghost-CNN ensures a lightweight architecture and low computational cost by replacing part of convolution operations with a series of linear transformations to generate ghost feature maps. Though the FLOPs of Ghost-NetVLAD is only 1% of that of VGG16-NetVLAD and its parameters is 17% of VGG16-NetVLAD's, Ghost-NetVLAD achieves similar accuracy with VGG16-NetVLAD. In addition, the amount of Ghost-NetVLAD's parameters is approximately half of that of MobileNetV3-NetVLAD and 75% of that of Alex-NetVLAD. Ghost-NetVLAD's performance is better than theirs.

4.4.3. Pre-train Experiment

From Table 3, Ghost-NetVLAD achieves better performance when GhostCNN is pre-trained on the Places-365 dataset. Compared with the ImageNet dataset, the Places-365 dataset includes more building categories, like museums and palaces, etc., while a small proportion is in the ImageNet dataset. Compared with the model pre-trained on the ImageNet dataset, the model pre-trained on Places-365 improves Recall@N by at least 5%. To explore the impact of pre-training level on the improvement of model accuracy, we pre-train the GhostCNN on Places-365 for different epochs. Top-1 accuracy shows an increasing trend as the increasing training epochs and Recall@N of Ghost-NetVLAD gets better. For the VPR problem, a specific pre-training process can make model accuracy become better. The possible reason is that CNN architecture learns from these building images to focus on more building features to improve the model performance since

Table 2

Recall@N of Alex-NetVLAD, VGG16-NetVLAD, MobileNetV3-NetVLAD, Ghost-NetVLAD and Ghost-dil-NetVLAD on the Pitts30k test dataset and TJU-Location test dataset. We report all results for each of them, including the **best** and **second-best** results.

Dataset	Model	recall@1	recall@5	recall@10	recall@20	recall@25
Pitts30k test	Alex-NetVLAD	69.87	85.02	89.14	92.52	93.81
	VGG16-NetVLAD	80.65	90.55	93.38	95.47	95.97
	MobileNetv3-NetVLAD	73.90	86.59	90.67	93.87	94.50
	Ghost-NetVLAD	68.54	82.83	87.50	91.73	92.63
	Ghost-dil-NetVLAD	79.45	89.67	92.80	95.35	95.95
TJU-Location test	Alex-NetVLAD	69.66	79.04	84.11	88.15	89.19
	VGG16-NetVLAD	72.01	79.04	82.42	88.15	89.32
	MobileNetV3-NetVLAD	69.01	77.08	81.77	86.59	88.15
	Ghost-NetVLAD	67.97	76.43	81.51	86.33	87.24
	Ghost-dil-NetVLAD	70.83	80.08	85.29	89.19	89.84

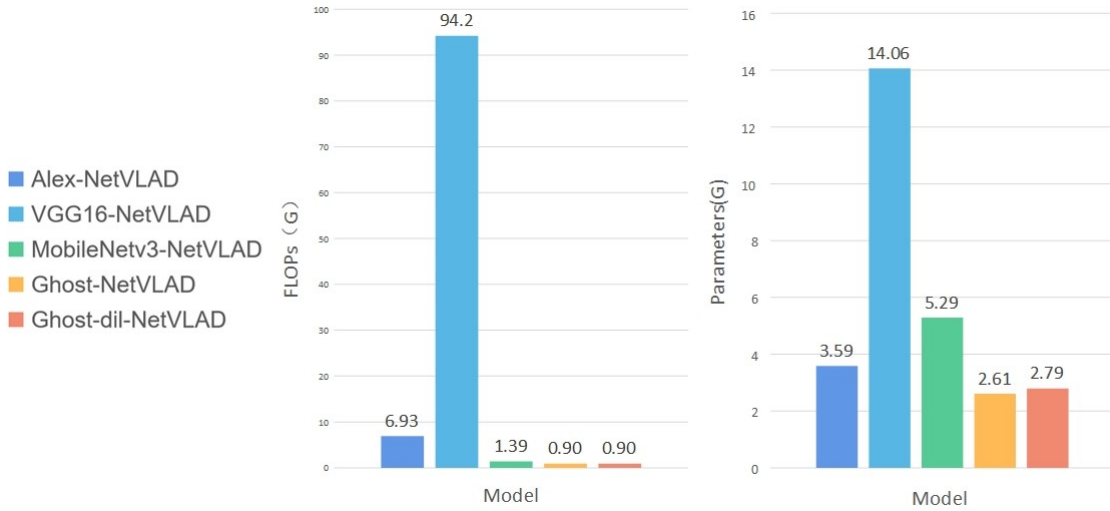


Figure 5: FLOPs and parameters of the Alex-NetVLAD, VGG16-NetVLAD, MobileNetV3-NetVLAD, Ghost-NetVLAD and Ghost-dil-NetVLAD.

Table 3

Recall@N of Ghost-NetVLAD on Pitts30k test dataset when GhostCNN is pre-trained on different datasets.

Dataset	Top-1 Acc.(%)	Recall@N		
		1	5	10
ImageNet	66.2	68.54	82.83	87.50
Places-365	43.84 (20 epochs)	76.38	87.88	91.34
	45.42 (30 epochs)	75.95	87.66	91.34
	46.52 (40 epochs)	76.03	86.59	90.67
	46.52 (60 epochs)	76.47	88.57	91.92

most scenes are full of buildings. Therefore, we think that the targeted pre-training process can help improve model accuracy.

4.4.4. GhostCNN with Dilated Convolution

Dilated convolution can expand the receptive field to get multi-scale context information. To further improve the accuracy of Ghost-NetVLAD, we try to apply dilated convo-

lutions to GhostCNN on the premise of not increasing the model size and training speed. We vary the dilated rate to validate our hypothesis. From Table 4, most Recall@N results for dilated rate>1 are greater than those of the model with dilated rate=1. The possible reason is the expanded receptive field brings more features and relationships among different objects. When the dilated rate is 5-2, the model achieves the best performance. After the first four stages of GhostCNN, the size of output feature map is 40×30. If we still choose a greater dilated rate for the last step, the receptive field may exceed the scope of the input feature map, bringing distortion of the output feature map.

5. Conclusions

In this paper, to improve the original NetVLAD, we proposes a lightweight model to make a good trade-off between accuracy and model efficiency. The experimental results show that the proposed model, Ghost-dil-NetVLAD (i.e., Ghost-NetVLAD with dilated convolutions), achieves similar accu-

Table 4

Recall@N of Ghost-NetVLAD with different dilated rates on Pitts30k test dataset. Dilated rate of a - b means that the dilated rate for first four stages of GhostCNN is a and b in the last stage.

Dataset	Dilated rate	Recall@N		
		1	5	10
Pitts30k test	1	76.38	87.88	91.34
	2	77.32	88.62	88.62
	3	78.08	88.03	91.45
	4	77.45	87.72	91.27
	5	78.24	89.39	92.56
	5-2	79.45	89.67	92.80
TJU-Location test	5-3	77.27	88.53	91.48
	1	70.31	76.17	82.42
	2	69.66	77.47	82.03
	3	67.45	77.86	83.33
	4	67.06	77.08	83.72
	5	68.75	78.52	84.51
	5-2	70.83	80.08	85.29
	5-3	68.23	76.56	82.55

racy with VGG16-NetVLAD and outperforms other mainstream NetVLAD-based methods because dilated convolutions may expand the receptive field to get more multi-scale context information. Meanwhile, our model reduces the FLOPs and parameters of VGG16-NetVLAD by 99.04% and 80.16%, respectively. In addition, the targeted pre-training process can help improve model accuracy efficiently.

Acknowledgments

This research is supported by National Natural Science Foundation of China (61771338). Thank Nanne *et al.* for implementing NetVlad in PyTorch (<https://github.com/Nanne/pytorch-NetVlad>). Thank Huawei Noah's Ark Lab for opening GhostNet in PyTorch (<https://github.com/huawei-noah/CV-Backbones>). Thank Dr Yixiao Ge at the Chinese University of Hong Kong (CUHK) for the discussion. Thank Chen Boxuan at Tianjin University for helping us collect the TJU-Location dataset images.

References

- [1] S. Lowry, N. Sünderhauf, P. Newman, J. J. Leonard, D. Cox, P. Corke, and M. J. Milford, "Visual place recognition: A survey," *IEEE Transactions on Robotics*, vol. 32, no. 1, pp. 1–19, 2015.
- [2] C. Masone and B. Caputo, "A survey on deep visual place recognition," *IEEE Access*, vol. 9, pp. 19 516–19 547, 2021.
- [3] M. Hussain, J. J. Bird, and D. R. Faria, "A study on cnn transfer learning for image classification," in *UK Workshop on computational Intelligence*. Springer, 2018, pp. 191–202.
- [4] A. Krizhevsky, I. Sutskever, and G. E. Hinton, "Imagenet classification with deep convolutional neural networks," *Advances in neural information processing systems*, vol. 25, pp. 1097–1105, 2012.
- [5] K. Simonyan and A. Zisserman, "Very deep convolutional networks for large-scale image recognition," *arXiv preprint arXiv:1409.1556*, 2014.
- [6] K. He, X. Zhang, S. Ren, and J. Sun, "Deep residual learning for im-

- age recognition," in *Proceedings of the IEEE conference on computer vision and pattern recognition*, 2016, pp. 770–778.
- [7] K. Han, Y. Wang, Q. Tian, J. Guo, C. Xu, and C. Xu, "Ghostnet: More features from cheap operations," in *Proceedings of the IEEE/CVF Conference on Computer Vision and Pattern Recognition*, 2020, pp. 1580–1589.
- [8] W.-L. Ku, H.-C. Chou, and W.-H. Peng, "Discriminatively-learned global image representation using cnn as a local feature extractor for image retrieval," in *2015 Visual Communications and Image Processing (VCIP)*. IEEE, 2015, pp. 1–4.
- [9] R. Arandjelovic, P. Gronat, A. Torii, T. Pajdla, and J. Sivic, "Netvlad: Cnn architecture for weakly supervised place recognition," in *Proceedings of the IEEE conference on computer vision and pattern recognition*, 2016, pp. 5297–5307.
- [10] X. Zhang, L. Wang, and Y. Su, "Visual place recognition: A survey from deep learning perspective," *Pattern Recognition*, vol. 113, p. 107760, 2021.
- [11] W. Zhou, H. Li, and Q. Tian, "Recent advance in content-based image retrieval: A literature survey," *arXiv preprint arXiv:1706.06064*, 2017.
- [12] R. Kapoor, D. Sharma, and T. Gulati, "State of the art content based image retrieval techniques using deep learning: a survey," *Multimedia Tools and Applications*, pp. 1–23, 2021.
- [13] A. Torii, J. Sivic, T. Pajdla, and M. Okutomi, "Visual place recognition with repetitive structures," in *Proceedings of the IEEE conference on computer vision and pattern recognition*, 2013, pp. 883–890.
- [14] A. Khaliq, S. Ehsan, Z. Chen, M. Milford, and K. McDonald-Maier, "A holistic visual place recognition approach using lightweight cnns for significant viewpoint and appearance changes," *IEEE transactions on robotics*, vol. 36, no. 2, pp. 561–569, 2019.
- [15] A. Khaliq, S. Ehsan, M. Milford, and K. McDonald-Maier, "Camal: Context-aware multi-scale attention framework for lightweight visual place recognition," 2019.
- [16] A. Babenko, A. Slesarev, A. Chigorin, and V. Lempitsky, "Neural codes for image retrieval," in *European conference on computer vision*. Springer, 2014, pp. 584–599.
- [17] I. Goodfellow, Y. Bengio, and A. Courville, *Deep learning*. MIT press, 2016.
- [18] M. Paulin, M. Douze, Z. Harchaoui, J. Mairal, F. Perronin, and C. Schmid, "Local convolutional features with unsupervised training for image retrieval," in *Proceedings of the IEEE international conference on computer vision*, 2015, pp. 91–99.
- [19] E. Mohamedano, K. McGuinness, N. E. O'Connor, A. Salvador, F. Marques, and X. Giró-i Nieto, "Bags of local convolutional features for scalable instance search," in *Proceedings of the 2016 ACM on International Conference on Multimedia Retrieval*, 2016, pp. 327–331.
- [20] J. Sánchez, F. Perronnin, T. Mensink, and J. Verbeek, "Image classification with the fisher vector: Theory and practice," *International journal of computer vision*, vol. 105, no. 3, pp. 222–245, 2013.
- [21] B. Cao, A. Araujo, and J. Sim, "Unifying deep local and global features for image search," in *European Conference on Computer Vision*. Springer, 2020, pp. 726–743.
- [22] J. Yu, C. Zhu, J. Zhang, Q. Huang, and D. Tao, "Spatial pyramid-enhanced netvlad with weighted triplet loss for place recognition," *IEEE transactions on neural networks and learning systems*, vol. 31, no. 2, pp. 661–674, 2019.
- [23] Y. Ge, H. Wang, F. Zhu, R. Zhao, and H. Li, "Self-supervising fine-grained region similarities for large-scale image localization," in *European Conference on Computer Vision*. Springer, 2020, pp. 369–386.
- [24] S. Hausler, S. Garg, M. Xu, M. Milford, and T. Fischer, "Patch-netvlad: Multi-scale fusion of locally-global descriptors for place recognition," in *Proceedings of the IEEE/CVF Conference on Computer Vision and Pattern Recognition*, 2021, pp. 14 141–14 152.
- [25] Y. Xu, J. Huang, J. Wang, Y. Wang, H. Qin, and K. Nan, "Esa-vlad: A lightweight network based on second-order attention and netvlad for loop closure detection," *IEEE Robotics and Automation Letters*, 2021.

- [26] A. G. Howard, M. Zhu, B. Chen, D. Kalenichenko, W. Wang, T. Weyand, M. Andreetto, and H. Adam, "Mobilenets: Efficient convolutional neural networks for mobile vision applications," *arXiv preprint arXiv:1704.04861*, 2017.
- [27] M. Sandler, A. Howard, M. Zhu, A. Zhmoginov, and L.-C. Chen, "Mobilenetv2: Inverted residuals and linear bottlenecks," in *Proceedings of the IEEE conference on computer vision and pattern recognition*, 2018, pp. 4510–4520.
- [28] A. Howard, M. Sandler, G. Chu, L.-C. Chen, B. Chen, M. Tan, W. Wang, Y. Zhu, R. Pang, V. Vasudevan *et al.*, "Searching for mobilenetv3," in *Proceedings of the IEEE/CVF International Conference on Computer Vision*, 2019, pp. 1314–1324.
- [29] X. Zhang, X. Zhou, M. Lin, and J. Sun, "Shufflenet: An extremely efficient convolutional neural network for mobile devices," in *Proceedings of the IEEE conference on computer vision and pattern recognition*, 2018, pp. 6848–6856.
- [30] N. Ma, X. Zhang, H.-T. Zheng, and J. Sun, "Shufflenet v2: Practical guidelines for efficient cnn architecture design," in *Proceedings of the European conference on computer vision (ECCV)*, 2018, pp. 116–131.
- [31] H. Jie, S. Li, and S. Gang, "Squeeze-and-excitation networks," in *2018 IEEE/CVF Conference on Computer Vision and Pattern Recognition (CVPR)*, 2018.
- [32] H. Jégou, M. Douze, C. Schmid, and P. Pérez, "Aggregating local descriptors into a compact image representation," in *2010 IEEE computer society conference on computer vision and pattern recognition*. IEEE, 2010, pp. 3304–3311.
- [33] H. Jégou and O. Chum, "Negative evidences and co-occurrences in image retrieval: The benefit of pca and whitening," in *European conference on computer vision*. Springer, 2012, pp. 774–787.
- [34] J. Deng, W. Dong, R. Socher, L.-J. Li, K. Li, and L. Fei-Fei, "Imagenet: A Large-Scale Hierarchical Image Database," in *CVPR09*, 2009.
- [35] K. He, R. Girshick, and P. Dollár, "Rethinking imagenet pre-training," in *Proceedings of the IEEE/CVF International Conference on Computer Vision*, 2019, pp. 4918–4927.
- [36] D. Hendrycks, K. Lee, and M. Mazeika, "Using pre-training can improve model robustness and uncertainty," in *International Conference on Machine Learning*. PMLR, 2019, pp. 2712–2721.
- [37] B. Zhou, A. Lapedriza, A. Khosla, A. Oliva, and A. Torralba, "Places: A 10 million image database for scene recognition," *IEEE transactions on pattern analysis and machine intelligence*, vol. 40, no. 6, pp. 1452–1464, 2017.